J|A|C|S
ARTICLES
Published on Web 03/01/2007

Search for a Predicted Hydrogen Bonding Motif − A Multidisciplinary Investigation into the Polymorphism of 3-Azabicyclo[3.3.1]nonane-2,4-dione

Ashley T. Hulme,[†] Andrea Johnston,[‡] Alastair J. Florence,[‡] Phillipe Fernandes,[‡] Kenneth Shankland,[§] Colin T. Bedford,[†] Gareth W. A. Welch,[†] Ghazala Sadiq,[∥] Delia A. Haynes,[⊥,#] W. D. Samuel Motherwell,[⊥] Derek A. Tocher,[†] and Sarah L. Price*[,†]

Contribution from the Christopher Ingold Laboratory, Department of Chemistry, University College London, 20 Gordon Street, London WC1H 0AJ, U.K., Strathclyde Institute of Pharmacy and Biomedical Sciences, 27 Taylor Street, University of Strathclyde, Glasgow G4 0NR, U.K., ISIS facility, CCLRC Rutherford Appleton Laboratory, Chilton, Didcot, Oxon OX11 1QX, U.K., Molecular Materials Centre, School of Chemical Engineering and Analytical Sciences, University of Manchester, Sackville Street, Manchester M60 1QD, U.K., and Cambridge Crystallographic Data Centre, 12 Union Road, Cambridge CB2 1EZ, U.K.

Received December 6, 2006; E-mail: s.l.price@ucl.ac.uk

Abstract: The predictions of the crystal structure of 3-azabicyclo[3.3.1]nonane-2,4-dione submitted in the 2001 international blind test of crystal structure prediction (CSP2001) led to the conclusion that crystal structures containing an alternative hydrogen bonded dimer motif were energetically competitive with the known catemer-based structure. Here we report an extensive search for a dimer-based crystal structure. Using an automated polymorph screen a new catemer-based metastable polymorph (form 2) and two new catemer-based solvates were found, and concurrent thermal studies reproduced form 2 and identified a plastic phase (form 3), whose powder X-ray diffraction pattern was consistent with the cubic space group $I2_3$ ($a = 7.5856(1)$ Å). Computational studies on the monomer showed that the imide N−H was a weak hydrogen bond donor, rationalizing the occurrence of the plastic phase which involved the breaking of all hydrogen bonds, and modeling of small clusters showed that dimers could easily reorganize to give the catemer. FTIR spectra confirmed the weakness of the hydrogen bond, with the solute showing no self-assembly in solution. It is concluded that the weakness of the N−H donor, coupled with the globular shape of the molecule, allows unusually facile transformation between alternative hydrogen bonding motifs during aggregation and nucleation.

Introduction

Computational methods of organic crystal structure prediction can only be definitively evaluated when all experimental polymorphs are known. The potential benefits of such computational methods to the pharmaceutical[1] and speciality chemicals industries, as well as fundamental scientific interest, have led the Cambridge Crystallographic Data Centre to organize three international blind tests of crystal structure prediction.[2−4] In the participants' discussion after the 2001 blind test[3] (CSP2001) it was observed that for two of the test molecules the predicted structures consistently showed a hydrogen bonding motif alternative to that found in the released experimental crystal structures. This led to the belief that there was the distinct potential for new polymorphs of these molecules to be discovered. For one of the two test molecules, the flexible molecule 6-amino-2-phenylsulfonylimino-1,2-dihydropyridine, a new polymorph was subsequently discovered with the expected alternative hydrogen bonding motif.[5] Here we report an extensive search for polymorphs of the second of these test molecules, the rigid molecule 3-azabicyclo[3.3.1]nonane-2,4-dione (**I**, Figure 1a).

From the results of CSP2001 it was found that the imide group of **I** could principally form two hydrogen bond motifs, an $R_2^2(8)$ dimer (Figure 1b) and a catemer (Figure 1c). In CSP2001 many of the participants had the same dimer-based structure within their three submitted crystal structure predictions, and it was even the first ranked structure submitted by

[†] University College London.
[‡] University of Strathclyde.
[§] CCLRC Rutherford Appleton Laboratory.
[∥] University of Manchester.
[⊥] Cambridge Crystallographic Data Centre.
[#] Current address: School of Chemistry, University of KwaZulu-Natal, Howard College Campus, Durban, 4041, South Africa.

(1) Price, S. L. *Adv. Drug Delivery Rev.* **2004**, *56*, 301−319.
(2) Lommerse, J. P. M.; Motherwell, W. D. S.; Ammon, H. L.; Dunitz, J. D.; Gavezzotti, A.; Hofmann, D. W. M.; Leusen, F. J. J.; Mooij, W. T. M.; Price, S. L.; Schweizer, B.; Schmidt, M. U.; van Eijck, B. P.; Verwer, P.; Williams, D. E. *Acta Crystallogr., Sect. B* **2000**, *56*, 697−714.
(3) Motherwell, W. D. S. et al. *Acta Crystallogr., Sect. B* **2002**, *58*, 647−661.
(4) Day, G. M. et al. *Acta Crystallogr., Sect. B* **2005**, *61*, 511−527.
(5) Jetti, R. K. R.; Boese, R.; Sarma, J.; Reddy, R. S.; Vishweshwar, P.; Desiraju, G. R. *Angew. Chem., Int. Ed.* **2003**, *42*, 1963−1967.

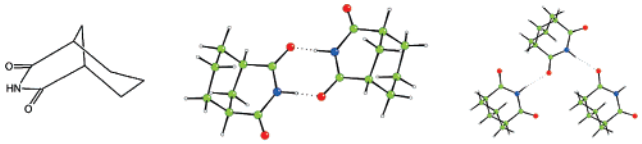

Figure 1. (a) Molecular diagram for 3-azabicyclo[3.3.1]nonane-2,4-dione (**I**); (b) a representative $R_2^2(8)$ dimer motif taken from a predicted structure; (c) the chain motif (found in form 1).

both of the participants who submitted the correct catemer-based structure (form 1) as their second and third choices, respectively.[3] The majority of submissions were based on a computational search for the global minimum in the lattice energy, which found a large number of both dimer- and catemer-based structures to be energetically competitive leading to the supposition that a polymorph of **I** could well exist based on the $R_2^2(8)$ dimer hydrogen bonding motif. An alternative crystal structure prediction method[6] compared a set of computationally generated crystal structures with a carefully chosen subset of the experimental crystal structures from the Cambridge Structure Database (CSD)[7] that contained the same imide functional group and concluded that the correct catemer-based structure was more likely to occur than dimer-based structures. With the implicit influence of any kinetic factors on the structures present in the CSD, this suggests[6] that there may be a kinetic reason why the catemer-based structure is observed.

I was synthesized in sufficient quantities (ca. 35 g) to perform an automated parallel solvent crystallization screen to discover alternative polymorphs of **I**, which could be based on the $R_2^2(8)$ dimer motif. We report the crystallization conditions that produced two solvates of **I** and the thermal methods that yielded two new polymorphs of **I**: a metastable catemer-based polymorph related to form 1[8] and a high-temperature plastic phase. Given that the extensive experimental searches failed to find the alternative dimer-based hydrogen bonding motif, further investigations were undertaken to determine the kinetic factors that preclude the formation of the dimer-based polymorphs for this molecule, while both dimer- and catemer-based polymorphs can be observed in other systems. The formation of the plastic phase suggests that hydrogen bonding in **I** is unusually weak for a N—H···O═C conventional hydrogen bond and easily disrupted, which was confirmed by examination of the electrostatic potential which showed that the N—H in the imide functional group is a weak hydrogen bond donor. Cluster calculations were used to explore the stability of the $R_2^2(8)$ dimers with respect to disruption by the introduction of further molecules, and from these it was concluded that the barrier to rearrangement from the dimer to catemer motifs is negligible. FTIR spectra of **I** in both polar and nonpolar solutions showed no self-assembly of molecules of **I**, for which strong hydrogen bonds would be required. Consequently, a rationalization for the lack of a dimer-based structure is developed by a combination of experimental and computational studies.

Method

Synthesis. A total of 37.7 g of 3-azabicyclo[3.3.1]nonane-2,4-dione was synthesized in a two-step process. The procedure of Goodwin and Perkin[9] was used to enrich mixed *cis*/*trans* 1,3-cyclohexanedicarboxylic acid to the pure *cis* acid. A modified version of the method of Hall[10] was used to give the final product. The powder X-ray pattern of the synthesized product was compared to the simulated powder pattern from the single-crystal structure[8] of form 1, and they were found to match. Full details are given in the Supporting Information.

Table 1. Outline of Conditions Included in the Automated Parallel Crystallization Search on **I**[a]

crystallization condition[b]	mass of solid added	crystallization method	agitation (rpm)
1	excess	cooling[c] to 288 K	1000
2	100 mg	cooling to 288 K	850
3	100 mg	evaporation	500

[a] Conditions 1 and 2 used the complete library of 67 solvents. Condition 3 used a reduced library of 48 solvents. [b] Solutions were prepared by adding solid to 2 mL of each solvent at the selected temperature (T_{prep}), prior to being filtered automatically into a clean crystallization vessel. Postdissolution, in-line filtration excludes undissolved particulates larger than 10 μm. A short heating cycle is then applied to the postfiltration solutions to remove smaller seeds before crystallization is induced. Condition 1, an excess of solid (typically >500 mg) was added such that the solution was saturated at T_{prep} (see Supporting Information for full details of individual crystallizations). Condition 2, 100 mg of **I** were added to each 2 mL of solvent at T_{prep} for each solvent group, varying the rate and extent of supersaturation obtained during cooling. For Condition 3, 100 mg of **I** were added to 2 mL of solvent at T_{prep} and heated solutions were transferred to clean glassware and held at elevated temperature with agitation. Recrystallization was then induced by evaporation. Evaporation temperatures for each solution ranged from 313 to 348 K depending on the solvent boiling point (see Supporting Information). [c] The cooling rate used for Conditions 1 and 2 was approximately 3.5 K min^{-1}. The solvent library (67 solvents, see Supporting Information for details) was ranked according to solvent boiling point and divided into four groups of ca. 16 solvents each. Within each solvent group, the temperature at which solutions were prepared (T_{prep}) is equivalent to T_{prep} = (minimum boiling point within group − 10) K.

Thermal Analysis and Capillary Variable-Temperature XRPD. The thermal properties of **I** were studied using a combination of hot-stage microscopy (HSM; Meiji Techno ML9430 polarizing microscope, with JVC color video camera and Linkam Scientific Instruments hot-stage with TMS 94 controller) and simultaneous differential scanning calorimetry (DSC) and thermogravimetric analysis (TGA) thermal analysis (STA; Netzsch STA 449-C Jupiter instrument). For STA analysis samples were placed in pierced 10 μL aluminum pans and heated from 298 to 473 K at 10 K min^{-1}.

Data for structural analysis were collected using variable-temperature capillary XRPD. Samples were lightly ground with an agate mortar and pestle and filled into 0.7 mm borosilicate glass capillaries prior to being mounted and aligned on a Bruker-AXS D8 Advance powder diffractometer. The instrument was equipped with transmission capillary geometry, a primary monochromator (Cu Kα_1; λ= 1.540 56 Å), and a Vantec position sensitive detector. The plastic phase of **I** was prepared in situ by heating a sample of form 1 to 420 K using an Oxford Cryosystems 700 Plus Series cryostream device. Form 2 was obtained by rapidly cooling the plastic phase from 420 to 250 K inside a 0.7 mm borosilicate glass capillary.

Automated Solvent Crystallization Screen. I was recrystallized from solution, using an automated parallel crystallization approach involving a total of 182 individual crystallizations implemented on a Chemspeed Accelerator SLT100 platform.[11,12] The search utilized a library of 67 solvents covering a diverse range of physicochemical properties. Crystallization was induced in filtered solutions by either controlled cooling or evaporation (Table 1). Upon recrystallization, suspended samples were reclaimed by filtration and transferred to a

(6) Sarma, J. A. R. P.; Desiraju, G. R. *Cryst. Growth Des.* **2002**, *2*, 93−100.
(7) Allen, F. H. *Acta Crystallogr., Sect. B* **2002**, *58*, 380−388.
(8) Howie, R. A.; Skakle, J. M. S. *Acta Crystallogr., Sect. E* **2001**, *57*, o822−o824.
(9) Goodwin, W.; Perkin, W. H. *J. Chem. Soc.* **1905**, *87*, 841−855.
(10) Hall, H. K., Jr. *J. Am. Chem. Soc.* **1958**, *80*, 6412−6420.
(11) Florence, A. J.; Johnston, A.; Price, S. L.; Nowell, H.; Kennedy, A. R.; Shankland, N. *J. Pharm. Sci.* **2006**, *95*, 1918−1930.
(12) Florence, A.; Johnston, A.; Fernandes, P.; Shankland, N.; Shankland, K. *J. Appl. Crystallogr.* **2006**, *39*, 922−924.

multiposition sample holder for sample identification using multisample foil transmission XRPD[13] (full experimental details are provided in the Supporting Information).

Solid State and Solution Infrared Spectroscopy. Solid state spectra of both **I** and succinimide were recorded at room temperature using a Perkin-Elmer Spectrum One FTIR-ATR spectrometer fitted with a diamond ATR crystal. Spectra of saturated solutions of **I** and succinimide in pentane, chloroform, water, and methanol were recorded at room temperature in ATR mode using an Atavar 360 ESP spectrometer fitted with a diamond composite ATR crystal in conjunction with Nicolet's OMNIC software. All solvents were spectroscopic grade.

Computational Modeling. The molecular structure was ab initio optimized at the MP2 6-31G(d,p) level, using Gaussian03.[14] This electron density was analyzed using GDMA2.2[15] to provide a distributed multipole description which was used to calculate the electrostatic contribution to the intermolecular potential, by including all terms in the atom−atom multipole series up to R_{ik}^{-5}. All other terms in the intermolecular potential were modeled by an isotropic atom−atom empirical potential:

$$U = \Sigma((A_\iota A_\kappa)^{1/2} \exp(-(B_\iota + B_\kappa)R_{ik}/2) - (C_\iota C_\kappa)^{1/2}/R_{ik}^6)$$

where atom i in molecule 1 is of type ι and atom k in molecule 2 is of type κ, using a set of parameters[16] for atomic types C, N, O, H_C, and H_N which had been derived by empirical fitting to a range of crystal structures and heats of sublimation.

This intermolecular potential energy surface was used in cluster calculations performed using ORIENT.[17] This program was also used to calculate the electrostatic potential arising from the distributed multipole model on the solvent accessible surface of **I**, defined as 1.4 Å above the van der Waals surface,[18] as defined by the Bondi radii[19] with a zero radius on the polar hydrogen atom (H_N).[20]

A representative crystal structure prediction search (see Supporting Information) was also carried out with this intermolecular potential, to confirm that, as in SLP's entry in CSP2001, it generated approximately equi-energetic dimer- and catemer-based crystal structures. The program MOLPAK[21] was used to generate densely packed hypothetical crystal structures using the same rigid ab initio optimized molecule conformation. The physical properties of this small, illustrative set of predicted crystal structures were also calculated: the elastic tensor and intermolecular phonons[22,23] were calculated in the rigid-body harmonic approximation and used to estimate[24] the free energy at 298 K; the morphologies of the low-energy crystals were estimated using the attachment energy model and used to estimate[25] the relative rates of growth of the different crystals from the vapor.

Most of the calculations were repeated using the distributed multipoles obtained from a PBE0[26] charge density calculated with a Sadlej basis set,[27] to test the sensitivity to variations in theoretically reasonable electrostatic models.[28]

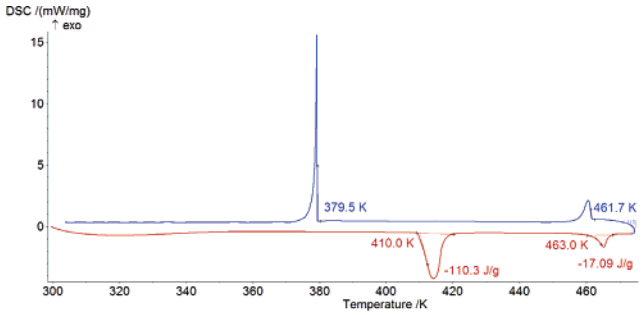

Figure 2. Differential scanning calorimetry data exhibiting the phase change to the plastic phase and the melting event. Heating was from 303 to 473 K at 10 K min^{-1} (red), followed by cooling back to 303 K at a rate of 10 K min^{-1} (blue).

Results

Thermal Analysis. DSC on form 1 identified an endotherm (410 K) prior to melting (463 K) which corresponds to a transition to a crystalline plastic phase, form 3 (Figure 2). HSM showed a loss of birefringence at ca. 418 K accompanying the transition with the crystallites retaining their morphology in the plastic state until a further increase in temperature gave rise to plastic flow (Figure 3). XRPD data for form 3 were indexed to give a cubic lattice (DICVOL-91[29]) which was confirmed by a Pawley-type fit[30] in TOPAS[31] to be consistent with a cubic lattice, space group $I2_13$, $a = 7.5856(1)$ Å, $V = 436.49(1)$ Å^3, $R_{wp} = 0.016$ (Figure 4). This represents a volume per molecule (218.25 Å^3) equivalent to a 15% increase on that for form 1 at 298 K. Cubic symmetry is characteristic of plastic crystals,[32,33] and the transition from an ordered crystal into a plastically crystalline state is usually accompanied by a decrease of 10−15% in density,[34] as such the body centered cubic structure is physically consistent with form 3 being a plastic crystal.

DSC analysis of the form 1 → form 3 transition based on seven repeats shows an average onset temperature of 408.6 ± 0.4 °C, giving $\Delta H_{trs} = 16.3 \pm 0.7$ kJ mol^{-1} and $\Delta S_{trs} = 39.9 \pm 1.9$ J K^{-1} mol^{-1}. For the form 3 melt, the average onset temperature from six measurements is 463.6 ± 0.3 °C, with $\Delta H_{fus} = 3.27 \pm 0.2$ kJ mol^{-1} and $\Delta S_{fus} = 7.05 \pm 0.43$ J K^{-1} mol^{-1}. Thus, this phase transformation satisfies a key thermodynamic criterion for plastic-crystal formation,[34] i.e., $\Delta S_{fus} <$ 21 J mol^{-1} K^{-1}, and has $\Sigma\Delta_{trs}S/\Delta_{fus}S = 5.7 > 1$.

Quench cooling a sample of form 3 held in a capillary from 425 to 245 K using a cryostream device produced a new metastable crystalline modification (form 2). The crystal structure was solved at 1.67 Å resolution by simulated annealing from laboratory powder data collected at 250 K. Subsequent Rietveld refinement yielded an R_{wp} of 0.070 to 1.54 Å

(13) Florence, A. J.; Baumgartner, B.; Weston, C.; Shankland, N.; Kennedy, A. R.; Shankland, K.; David, W. I. F. *J. Pharm. Sci.* **2003**, *92*, 1930−1938.
(14) Frisch, M. J., et al. *Gaussian 03*; Gaussian Inc.: Wallingford, CT, 2003
(15) Stone, A. J. *J. Chem. Theory Comput.* **2005**, *1*, 1128−1132.
(16) Coombes, D. S.; Price, S. L.; Willock, D. J.; Leslie, M. *J. Phys. Chem.* **1996**, *100*, 7352−7360.
(17) Stone, A. J.; Dullweber, A.; Engkvist, O.; Fraschini, E.; Hodges, M. P.; Meredith, A. W.; Nutt, D. R.; Popelier, P. L. A.; Wales, D. J. *ORIENT*, version 4.6; University of Cambridge: 2006
(18) Lee, B.; Richards, F. M. *J. Mol. Biol.* **1971**, *55*, 379.
(19) Bondi, A. *J. Phys. Chem.* **1964**, *68*, 441−451.
(20) Buckingham, A. D.; Fowler, P. W. *Can. J. Chem.* **1985**, *63*, 2018−2025.
(21) Holden, J. R.; Du, Z. Y.; Ammon, H. L. *J. Comput. Chem.* **1993**, *14*, 422−437.
(22) Day, G. M.; Price, S. L.; Leslie, M. *J. Phys. Chem. B* **2003**, *107*, 10919−10933.
(23) Day, G. M.; Price, S. L.; Leslie, M. *Cryst. Growth Des.* **2001**, *1*, 13−26.
(24) Anghel, A. T.; Day, G. M.; Price, S. L. *CrystEngComm* **2002**, *4*, 348−355.
(25) Coombes, D. S.; Catlow, C. R. A.; Gale, J. D.; Rohl, A. L.; Price, S. L. *Cryst. Growth Des.* **2005**, *5*, 879−885.
(26) Adamo, C.; Barone, V. *J. Chem. Phys.* **1999**, *110*, 6158−6170.
(27) Sadlej, A. J. *Collect. Czech. Chem. C* **1988**, *53*, 1995−2016.
(28) Misquitta, A. J.; Szalewicz, K. *J. Chem. Phys.* **2005**, *122*, art-214103.
(29) Boultif, A.; Louër, D. *J. Appl. Crystallogr.* **1991**, *24*, 987−993.
(30) Pawley, G. S. *J. Appl. Crystallogr.* **1981**, *14*, 357−361.
(31) Coelho, A. A. *Topas user manual*, version 3.1 ed.; Bruker AXS GmbH: Karlsruhe, Germany, 2003.
(32) Dunning, W. J. *J. Phys. Chem. Solids* **1961**, *18*, 21−27.
(33) Dunning, W. The Crystal Structure of Some Plastic and Related Crystals. In *Plastically Crystalline State: Orientationally Disordered Crystals*; Sherwood, J. N., Ed.; John Wiley & Sons: Chichester, 1979; pp 1−37.
(34) Bazyleva, A. B.; Kabo, G. J.; Blokhin, A. V. *Physica B* **2006**, *383*, 243−252.

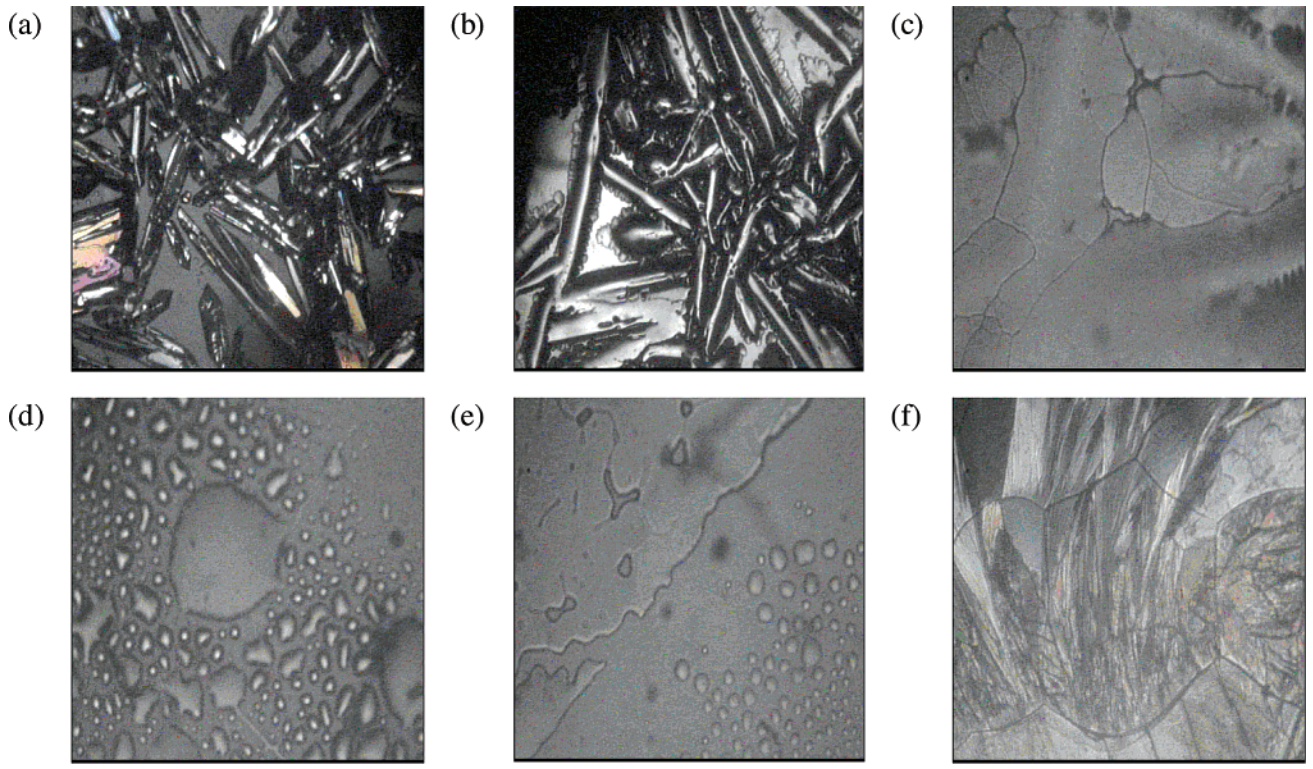

Figure 3. Hot stage microscopy: (a) crystals of form 1 at room temperature; (b) plastic phase at 418 K; (c) on further heating plastic flow is observed; (d) melting of plastic phase at 468 K; (e) liquid droplets condense to plastic phase below 463 K; (f) plastic phase converts to form 1 at 381 K.

resolution.[35] Form 2 contains two molecules in the asymmetric unit and has a unit cell that closely approximates that of form 1 doubled along the *c*-axis and may well be an example of a metastable form which represents a stage in the pathway from the plastic phase toward the more stable form 1.[36] Indeed, on standing, form 2 transforms fully to form 1 within an hour at room temperature, showing this to be an example of a higher Z′ metastable polymorph, with pseudo-symmetry, that converts readily to a more stable lower Z′ form.[37] Form 2 was also recrystallized from solution, though from only two of the solvents used in the search (see below).

Automated Solvent Crystallization Screen. The automated solvent screen produced 172 crystalline samples from the total of 182 crystallization experiments. The condition and outcome of each individual crystallization is given in the Supporting Information. In summary, the majority (162/172) of crystallizations gave the known form 1, two crystallizations (from CCl_4 and $CHCl_3$ under condition 1, Table 1) gave the metastable form 2, and acetic acid (3/172) and 1-methylnapthalene (2/172) each yielded novel solvates. The structure of the acetic acid solvate[38] was solved by single-crystal X-ray diffraction from block crystals obtained from one of the automated crystallizations. However, the 1-methylnapthalene solvate grew as fine needles and was only suitable for structure solution by simulated annealing from laboratory capillary XRPD data,[39] collected at room temperature. Subsequent Rietveld refinement, using data collected to 1.51 Å resolution, yielded an R_{wp} value of 0.057.

The hydrogen bonding motifs in the two solvate structures and polymorphic forms 1 and 2 are shown in Figure 5. The chain in form 2 is visually similar to that in form 1, but the glide symmetry that propagates the form 1 chain is lost in the form 2 chain with two symmetry independent molecules in the unit cell. The chains lie side by side forming layers in both forms, but form 1 has an ABAB layer repeat, whereas form 2 has an ABCD repeat, with CD related to AB by a shift of approximately half a unit cell (Supporting Information Figure S8). The chain of molecules of **I** in the 1-methylnapthalene solvate is very similar to that found in both polymorphs, with six chains surrounding channels of 1-methylnaphthalene molecules. The acetic acid solvate crystal structure has the solvent incorporated into the catemer motif with the carboxylic acid group mimicking the role of the CO−NH group of **I** in the chain structure.

Discussion of the Experimental Polymorph Screen. The automated crystallization search found a metastable polymorph (form 2) and two solvates; however all three crystal structures are based on the hydrogen bonded catemer motif, and no evidence of $R_2^2(8)$ dimer-based structures was found. The search was designed to test the effect of a wide range of solvent properties, supersaturation, temperature, and agitation on the crystallization of **I** while eliminating seeding by the raw material (form 1). Rapid crystallization was obtained by controlled cooling (Table 1) and may favor the formation of metastable forms (i.e., kinetic conditions), while the variation in solvent and concentration may influence the mode of association of molecules of **I** in solution prior to nucleation. However, if a

(35) Hulme, A. T.; Fernandes, P.; Florence, A.; Johnston, A.; Shankland, K. *Acta Crystallogr., Sect. E* **2006**, *62*, o3046−o3048.
(36) Mondal, R.; Howard, J. A. K. *CrystEngComm* **2005**, *7*, 462−464.
(37) Anderson, K. M.; Afarinkia, K.; Yu, H. W.; Goeta, A. E.; Steed, J. W. *Cryst. Growth Des.* **2006**, *6*, 2109−2113.
(38) Hulme, A. T.; Johnston, A.; Florence, A. J.; Tocher, D. A. *Acta Crystallogr., Sect. E* **2006**, *62*, O545−O547.
(39) Hulme, A. T.; Fernandes, P.; Florence, A.; Johnston, A.; Shankland, K. *Acta Crystallogr., Sect. E* **2006**, *62*, o3752−o3754.

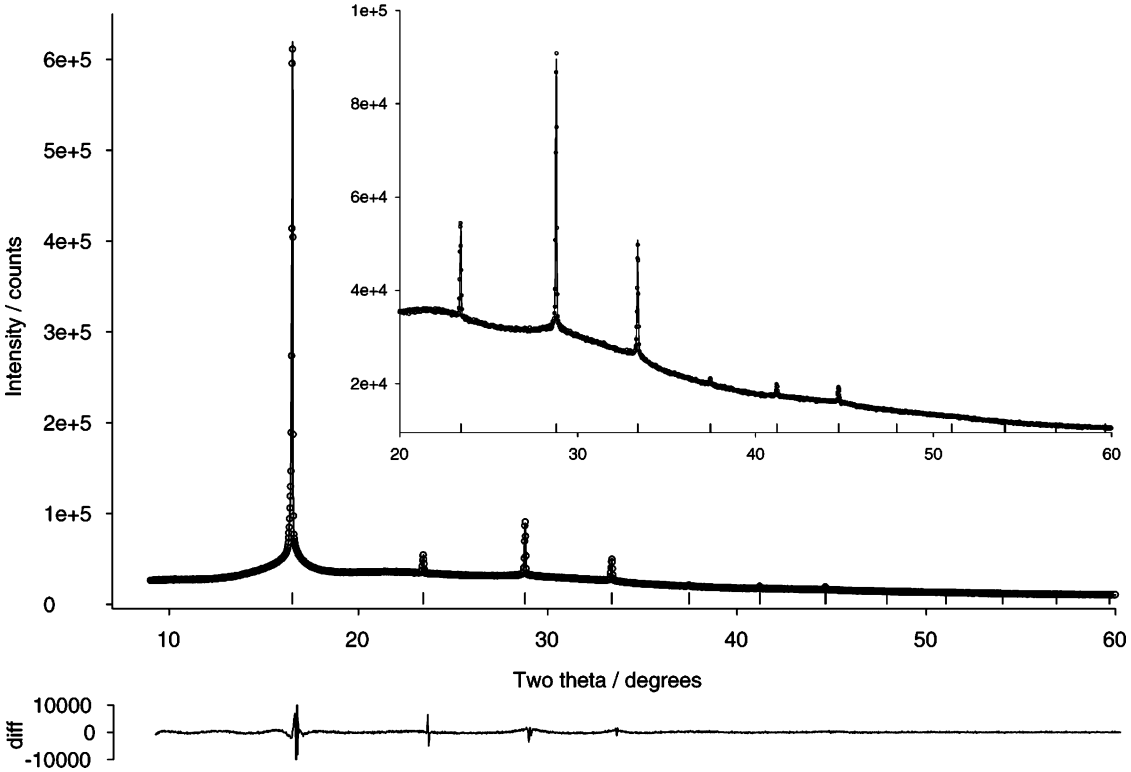

Figure 4. Final observed (○), calculated (—), and difference ($y_{obs} - y_{calc}$) profiles for the Pawley-type fit to capillary XRPD data collected from a sample of the plastic crystalline phase (form 3) in the range 9°−60° 2θ. Inset, zoomed plot showing the fit to the data in the range 20°−60° 2θ. The pattern is consistent with that expected from a disordered cubic plastic phase with relatively few observed peaks across the full data range and considerable background scattering. The observed misfit in the final refinement is attributable to small inaccuracies in modeling both the background and the peak shape for reflections belonging to the cubic cell.

highly metastable dimer-based structure was formed as the first emergent phase under any of the conditions tested, it either did not survive past critical-nucleus size[40] or transformed via either solution-mediated or solid−solid transformation prior to XRPD detection. Variable temperature XRPD studies plus complementary sublimation and high-pressure crystallization from solvent[41] were also unsuccessful in producing any evidence of additional polymorphs. From this extensive experimental search, it appears most unlikely that an $R_2^2(8)$ dimer-based polymorph of **I** can be formed by the growth of crystals from the gas phase or solution.

Infrared Solid State and Solution Spectra. Infrared spectra of **I** in various solutions and the solid state were carried out to attempt to exploit the emerging link between structural synthons present in the crystal structure and the growth synthons present in solution from self-association equilibria.[42] An indication of whether a dimer-based structure of **I** could ever be found would be the observation of self-assembled dimer units in solution, most likely in nonpolar solutions. The $R_2^2(8)$ carboxylic acid dimer motif has been shown by infrared spectroscopy to be present in chloroform solutions of tetrolic and benzoic acid, which crystallize to give structures containing the dimer motif, and absent in the ethanolic solutions of tetrolic acid which give rise to the catemeric β-polymorph of tetrolic acid.[43] Solutions of **I** in pentane and chloroform were studied because these solvents were likely to promote the formation of $R_2^2(8)$ dimers in the solution. For comparison, spectra of solutions in methanol and water were also recorded, as these solvents could be expected to solvate **I** more strongly and disrupt any self-assemblies. Given the solid state spectrum of **I**, it was expected that a strongly hydrogen bonded carbonyl bond would absorb at around 1680−90 cm^{-1}. However, the infrared spectra of **I** in pentane, methanol, and water showed no significant differences from one another with the carbonyl frequency recorded at approximately 1740 cm^{-1} in all solutions indicating that **I** is monomeric in all cases. In chloroform, a shift of the carbonyl frequency to 1706 cm^{-1} is only suggestive of solvation rather than dimerization. Hence, it seems that **I** does not associate in solution and the $R_2^2(8)$ motif remains unobserved. The infrared spectra of succinimide, a molecule that forms the $R_2^2(8)$ dimer in the crystalline state,[44] were measured for the solid state and the same four solvents, and it also appears to be monomeric in solution. Since succinimide crystallizes as a dimer, it can only be concluded that the lack of dimers of **I** in solution does not preclude the formation of a dimer in developing crystal nuclei. The solution and solid state infrared spectra are included in the Supporting Information.

Cluster Modeling and Crystal Structure Prediction. Further evidence of the weakly interacting nature of molecules of **I** in $R_2^2(8)$ dimers comes from energy minimization of clusters of three or four molecules using the distributed multipole intermolecular potential. Figure 6 shows one particularly sug-

(40) Davey, R. J.; Allen, K.; Blagden, N.; Cross, W. I.; Lieberman, H. F.; Quayle, M. J.; Righini, S.; Seton, L.; Tiddy, G. J. T. *CrystEngComm* **2002**, *4*, 257−264.
(41) Wood, P. A.; Parsons, S.; Pidcock, E. 2005. Personal Communication.
(42) Hunter, C. A. *Angew. Chem., Int. Ed.* **2004**, *43*, 5310−5324.
(43) Davey, R. J.; Dent, G.; Mughal, R. K.; Parveen, S. *Cryst. Growth Des.* **2006**, *6*, 1788−1796.
(44) Mason, R. *Acta Crystallogr.* **1961**, *14*, 720−724.
(45) Schaftenaar, G.; Noordik, J. H. *J. Comput. -Aided Mol. Des.* **2000**, *14*, 123−134.

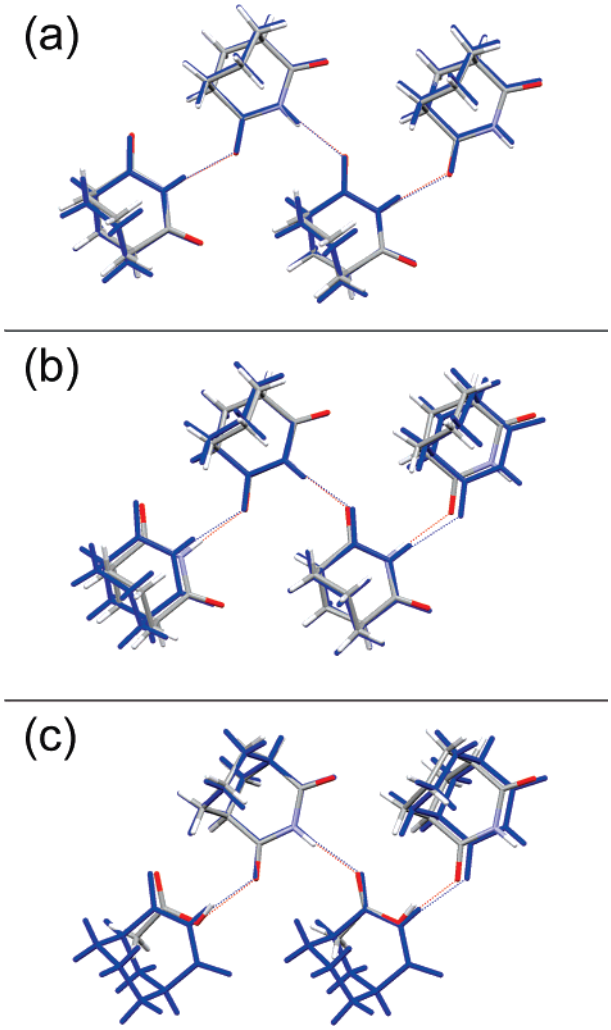

Figure 5. Hydrogen-bonded chains of **I** in form 1 (blue) overlaid with those in (a) form 2; (b) the methylnaphthalene solvate and (c) the acetic acid solvate.

gestive trajectory that provides some understanding of the crystallization pathway of **I**: a third molecule readily hydrogen bonds to the unused acceptor of a previously optimized $R_2^2(8)$ dimer (Figure 6 step 1 to 2). The energy is lowered by rearrangement of the molecules (to step 3), and finally a small energy lowering is achieved by tilting the hydrocarbon moieties into better van der Waals contact (step 3 to 4), although this involves breaking a hydrogen bond, resulting in a hydrogen-bonding chain motif for the trimer (4). The optimized trimer has gained 12.1 kJ mol^{-1} in dispersion energy and lost 6.5 kJ mol^{-1} in electrostatic energy relative to the intermediate trimer cluster with the $R_2^2(8)$ motif (3), which is only 2.0 kJ mol^{-1} less stable.

The tendency for the approach of other molecules to disrupt or severely distort the hydrogen bonding of the $R_2^2(8)$ dimer occurred in 5 of the 20 optimizations attempted, including one where two $R_2^2(8)$ dimers were allowed to approach one another. When the alternative potential energy surface with a stronger electrostatic interaction was used,[28] the occurrence of trajectories that led to the breakage of the dimer hydrogen bonding was reduced, though not precluded. This is consistent with there being a subtle balance between the electrostatic and dispersion forces between molecules of **I** that produces some

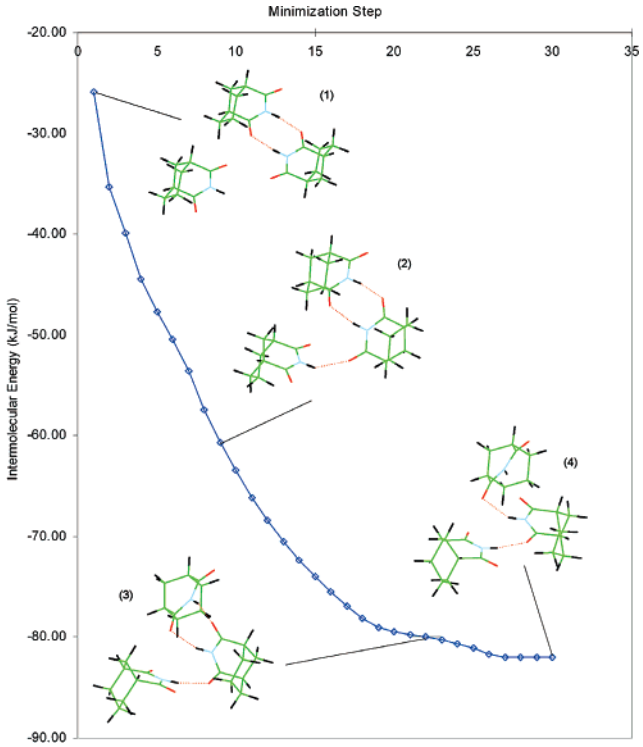

Figure 6. An optimization of the intermolecular energy of three molecules of **I**. The inset molecular diagrams show the conformation at the indicated steps, starting from a dimer and a monomer, formation of a hydrogen bond between the monomer proton and a free oxygen in the dimer, and further rearrangement of the trimer to reach a minimum on the intermolecular potential energy surface. Dotted red lines indicate hydrogen bonds defined by 1.5 < H···O < 3.15 Å and N−H···O > 145° as given by MOLDEN.[45]

clusters with chain hydrogen bonds of lower energy than those with the $R_2^2(8)$ hydrogen bonding motif.

Both of the intermolecular potentials predict approximately equienergetic dimer- and catemer-based crystal structures, with a dimer-based global minimum (Table 2). Forms 1 and 2 are only about 0.5 kJ mol^{-1} above the global minimum, although this increases to 2 kJ mol^{-1} for the alternative molecular charge density model,[28] which has a larger electrostatic contribution to the lattice energy of approximately 10 kJ mol^{-1}. A comparison with a selection of published computational models for the lattice energy of predicted structures of **I** (Table 2) shows that form 1 is generally only slightly less stable than hypothetical dimer structures. Although not one of these intermolecular potential models explicitly includes the induction energy, the success of this type of model in crystal structure predictions of related molecules[46] and some preliminary estimates of the induction contribution[47] show that the distortion of the charge density within the crystal lattice is unlikely to make the dimer-based structures thermodynamically unfeasible. The calculated lattice energies refer to static crystal structures at 0 K; however the harmonic rigid-body crystal lattice modes and elastic constants of the dimer- and chain-based low-energy structures do not give a significant difference in the estimated free energies at room temperature (Table 3). Thus given the uncertainties of

(46) Day, G. M.; Motherwell, W. D. S.; Jones, W. *Cryst. Growth Des.* **2005**, *5*, 1023−1033.
(47) Welch, G. W. A. 2006. Personal Communication.
(48) Williams, D. E. *J. Mol. Struct.* **1999**, *486*, 321−347.
(49) Williams, D. E. *J. Comput. Chem.* **2001**, *22*, 1154−1166.
(50) Mayo, S. L.; Olafson, B. D.; Goddard, W. A. *J. Phys. Chem.* **1990**, *94*, 8897−8909.

Table 2. Comparison of the Relative Stability of the Known and Hypothetical Crystal Structures of **I** in a Range of Crystal Structure Predictions by Lattice Energy Minimization[a]

repulsion–dispersion model	electrostatic model	reference	global minimum motif	rank, ΔE kJ mol^{-1} form 1	rank, ΔE kJ mol^{-1} form 2
FIT[16]	multipoles (MP2, 6-31G**)	this work	dimer	**5**, 0.6	**4**, 0.5
FIT[16]	multipoles (PBE0, Sadlej)	this work	dimer	**5**, 1.9	**9**, 2.1
Will99[48,49]	multipoles (DFT B3P91)	46	chain = dimer (∼ak98)	**3**, 0.15	
Will99[48,49]	charges (DFT B3P91)	46	dimer (∼ak98)	**7**, 3.37	
CVFF	charges	Leusen[3]	dimer (∼ak98)	**3**, 0.5	
Dreiding[50]	multipoles	Mooij[3]	dimer (∼ak98)	**2**, 0.2	

[a] Only the two submissions in CSP2001 which found the correct chain structure are included, but seven other submissions with different energy models had a dimer-based structure that approximates ak98 (Table 3) in their three submissions (see Table 9 in ref 3).[3]

Table 3. Properties of Crystal Structures of **I** Corresponding to the Lowest Lattice Energy Minima[a]

structure	space group	Z	*a* (Å)	*b* (Å)	*c* (Å)	β (deg)	density (g/cm^3)	growth rate[b]	lowest shear[c] (GPa)	free energy[d] (kJ/mol)	lattice energy (kJ/mol)
cb33	*Pbca*	*8*	*11.5221*	*12.0423*	*11.4634*	*90.0*	*1.2793*	*376.26*	*2.9237*	*−106.146*	*−88.91*
aq15	$P2_12_12_1$	4	7.6543	12.2517	8.344	90.0	1.3002	309.47	5.7371	−104.934	−88.49
ak98	$P2_1/c$	*4*	*10.1991*	*7.8806*	*9.9281*	*76.8*	*1.3095*	*216.94*	*5.746*	*−104.968*	*−88.46*
form 2[e]	$P2_1/c$	**8**	**8.0295**	**10.3377**	**18.8224**	**95.9**	**1.3095**		**0.4119**	**−106.034**	**−88.40**
form 1[e]	$P2_1/a$	**4**	**7.8925**	**10.5992**	**9.3397**	**94.3**	**1.3059**	**232.19**	**2.4932**	**−105.041**	**−88.35**
am63	$P2_1/n$	*4*	*6.0716*	*11.5367*	*11.8665*	*76.9*	*1.2567*	*237.67*	*1.6561*	*−106.692*	*−87.69*
am22	$P2_1/n$	*4*	*6.2792*	*11.6268*	*11.1493*	*80.3*	*1.2683*	*228.72*	*0.3696*	*−105.656*	*−87.66*
am10	$P2_1/n$	*4*	*6.1566*	*11.4942*	*11.3872*	*80.5*	*1.2803*	*253.93*	*5.2291*	*−105.203*	*−87.49*

[a] Structures based on the $R_2^2(8)$ dimers are given in italics, and experimental structures, in bold. [b] The relative volume growth rate of the crystals calculated by assuming that the growth rate of every face is proportional to the attachment energy. This is not calculated for form 2 which has $Z' = 2$ and so a different growth unit. [c] The lowest eigenvalue of the shear submatrix of the elastic stiffness tensor. [d] Estimated Helmholtz free energy at 298 K as the sum of the thermal energy at 298 K, the lattice energy, and the zero-point vibrational energy, derived from second derivative properties for rigid body motions. [e] The experimental cell parameters which lead to this lattice energy minimum are *a*, *b*, *c* (Å) = 7.676, 10.594, 19.020; α, β, γ (deg) = 90.00, 94.125, 90.00 ($P2_1/c$) for form 2 and *a*, *b*, *c* (Å) = 7.677, 10.584, 9.311; α, β, γ (deg) = 90.00, 94.968, 90.00 ($P2_1$/a) for form 1. The relationship between the cells is given in the Supporting Information, Figure S8.

current computational models, it is plausible that form 1 is the thermodynamically most stable form but dimer-based structures are unlikely to be outside the energy range of possible polymorphism.

A prediction of the relative growth rate of the low-energy crystals from the vapor does show some variation between the structures (Table 3) but does not suggest that the surfaces of the dimer-based crystals, such as ak98, have particularly low attachment energies. Hence once the crystallites have formed, their relative growth rates, according to the simple attachment energy model, do not discriminate between chain- and dimer-based structures. The mechanical stabilities of the possible structures of **I** vary considerably (Table 3), with both chain- and dimer-based structures showing a wide range of anisotropy in their elastic constants. Form 2 is predicted to be particularly readily distorted by shearing forces, which is consistent with the ease of transformation of form 2 to form 1 by shifting of the layers. The lowest eigenvalue of the shear submatrix of 0.4 GPa for form 2 of **I** is somewhat larger than that of 0.15 GPa for a predicted structure of aspirin[51] that was subsequently found as a highly metastable polymorph.[52] However, the predicted dimer-based crystal structures are generally more mechanically stable. Thus, consideration of the properties of low-energy crystal structures for **I** does not give any reason why the catemer- and not the dimer-based structures are actually observed.

Discussion

Form 3 is an example of a novel plastic crystalline phase. Molecules with similar globular shapes,[53] such as bicyclo[3.3.1]-nonane,[54] bicyclo[3.3.1]nonan-9-one,[55] and 3-oxabicyclo[3.3.1]-nonane-2,4-dione, also form plastic phases, though not one of these molecules is capable of hydrogen bonding. Relatively few compounds containing hydrogen bond donors and acceptors are known to form plastic crystals with examples including cyclo-hexanol, trimethylacetic acid, and pentaerythritol derivatives.[33] In plastic crystals, it has long been accepted[53] that the molecules have the freedom to rotate while maintaining a coherent crystal lattice, until this is finally disrupted by melting, but only the most spherical molecules can approximate free rotation in the plastic phase. In most cases, the plastic crystal is "considered to be disordered: in different sites the molecules occupy one of *n* possible orientations and perform librations in the potential well accompanied by jumps from one equilibrium position to another".[56] In form 3, the body centered cubic structure implies a spherical molecule radius of 3.28 Å. The van der Waals surface

(51) Ouvrard, C.; Price, S. L. *Cryst. Growth Des.* **2004**, *4*, 1119−1127.
(52) Vishweshwar, P.; McMahon, J. A.; Oliveira, M.; Peterson, M. L.; Zaworotko, M. J. *J. Am. Chem. Soc.* **2005**, *127*, 16802−16803.
(53) Timmermans, J. *J. Phys. Chem. Solids* **1961**, *18*, 1−8.
(54) Laszlo, I. *Recl. Trav. Chim. Pays-Bas* **1965**, *84*, 251.
(55) Mora, A. J.; Fitch, A. N. *Z. Kristallogr.* **1999**, *214*, 480−485.

of **I** ranges from 2.1 to 4.3 Å from the center of mass, and so the molecules in form 3 must correspond to the jumping molecular disorder model. This model[57] could be used to estimate the number of discrete orientations in the plastic and ordered phases, $\Delta S_{trs} = R \ln(n_{plastic}/n_{ordered})$, with form 3 calculated to have 120 ± 30 discrete orientations. This is comparable with the estimated number of states for heptacyclotetradecane.[58] While there is little evidence that the entropies of transitions for molecular crystals correspond well to this model[59] and more sophisticated treatments are possible,[58] the large transition entropy is not compatible with a limited number of hydrogen bonding orientations. Thus, the structure and thermodynamics of formation of form 3 imply that the hydrogen bonding in the crystalline form 1 is significantly disrupted on forming the plastic phase.

If a dimer-based structure of **I** were ever to be formed, subsequent transformation to a more stable catemer-based structure would require a significant change in the hydrogen bonding. There is generally expected to be a significant energy barrier for the rearrangement of hydrogen bonds within the solid state, as many pairs of polymorphs which differ in their hydrogen bonding occur (e.g., tetrolic acid,[60] 5-fluorouracil,[61] famotidine,[62−64] and cimetidine[65]). However, for **I**, the thermal transition of form 1 to form 3 in which the hydrogen bonded chain cannot remain intact, allied to the globular shape of the molecule which allows its easy rotation, suggests that the barrier to hydrogen bond rearrangement in **I** may be unusually low.

The cluster calculations provide further evidence to support this hypothesis. The $R_2^2(8)$ dimer has an interaction energy of −36.3 kJ mol^{-1}, which is rather smaller than would be traditionally associated with two independent N−H···O=C hydrogen bonds.[66] This can be attributed to the proximity of the two carbonyls to the N−H group in the imide group reducing the electrostatic potential in the region of the donor (Figure 7) so that it is comparable with the potential in some of the purely hydrocarbon regions. This interplay of adjacent N−H and C=O groups has been shown to reduce the hydrogen bond strength[67] for barbituric acid, cyanuric acid, parabanic acid, and alloxan, which, when combined with steric considerations, leads to unused hydrogen bond acceptors in the crystal structures. Figure 7 also shows that **I** is also approximately spherical, and so, with the weak positive electrostatic potential around the imide proton, neither the steric nor electrostatic forces would produce a significant barrier to the rearrangement of the hydrogen bonds of **I**. Thus, loose prenucleation clusters of **I** are expected to have considerable freedom to rearrange to give the most stable crystal structure, almost certainly the catemer-based form 1, with the metastable form 2 a trapped intermediate showing the later stages of crystal organization[36] with chains forming early on in the nucleation process.

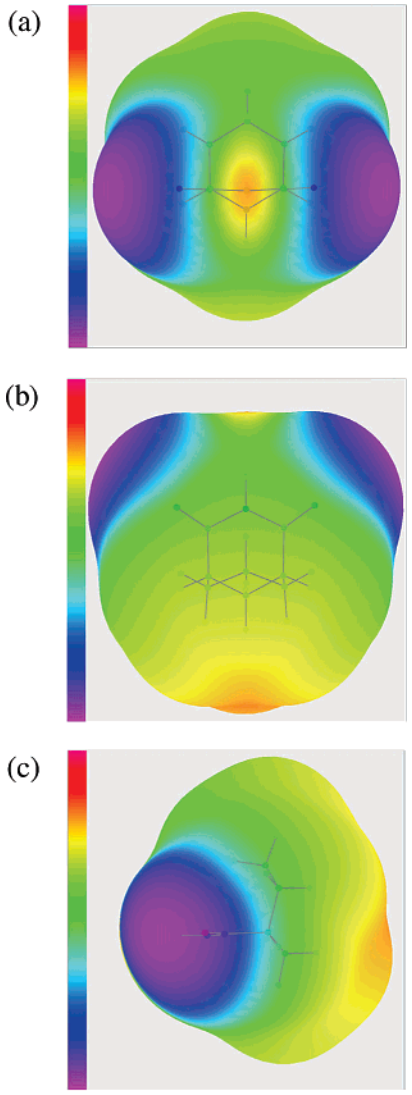

Figure 7. Electrostatic potential on the water-accessible surface of **I**. The color scale is from −60 to +60 kJ mol^{-1}; the minimum potential on this surface is −56.27 kJ mol^{-1}, and the maximum is +38.62 kJ mol^{-1}. The molecule is viewed (a) with the imide proton pointing directly out of the plane of the page; (b) from the side of the cyclohexane ring with the imide group vertical and slightly behind; and (c) perpendicular to the plane of symmetry.

While formation of a chain trimer shown in Figure 6 only approximates a possible path for molecular association from a gas at 0 K, the kinetic energy and possible solvent involvement in molecular association in real crystallization processes are likely to readily facilitate rearrangement of any $R_2^2(8)$ dimers into the more stable chains. The lack of FTIR spectroscopic evidence for dimers in even pentane solutions is consistent with the hydrogen bonding being so weak that $R_2^2(8)$ dimer formation of **I** is a rare event under any crystallization condition.

Conclusion

The extensive experimental screen undertaken has covered solvent and thermal crystallization methods without finding any

(56) Fouret, R. Diffuse X-Ray Scattering by Orientationally-Disordered Crystals. In *Plastically Crystalline State: Orientationally Disordered Crystals*; Sherwood, J. N., Ed.; John Wiley & Sons: Chichester, 1979; pp 85−121.
(57) Guthrie, G. B.; Mccullough, J. P. *J. Phys. Chem. Solids* **1961**, *18*, 53−61.
(58) Kabo, G. J.; Blokhin, A. V.; Charapennikau, M. B.; Kabo, A. G.; Sevruk, V. M. *Thermochim. Acta* **2000**, *345*, 125−133.
(59) Clark, T.; Mckervey, M. A.; Mackle, H.; Rooney, J. J. *J. Chem. Soc., Faraday Trans. 1* **1974**, *70*, 1279−1291.
(60) Leiserowitz, L.; Nader, F. *Angew. Chem., Int. Ed.* **1972**, *11*, 514−&.
(61) Hulme, A. T.; Price, S. L.; Tocher, D. A. *J. Am. Chem. Soc.* **2005**, *127*, 1116−1117.
(62) Ferenczy, G. G.; Parkanyi, L.; Angyan, J. G.; Kalman, A.; Hegedus, B. *THEOCHEM* **2000**, *503*, 73−79.
(63) Golic, L.; Djinovic, K.; Florjanic, M. *Acta Crystallogr., Sect. C* **1989**, *45*, 1381−1384.
(64) Shankland, K.; McBride, L.; David, W. I. F.; Shankland, N.; Steele, G. *J. Appl. Crystallogr.* **2002**, *35*, 443−454.
(65) Hegedus, B.; Gorog, S. *J. Pharm. Biomed. Anal.* **1985**, *3*, 303−313.
(66) Desiraju, G. R. *Acc. Chem. Res.* **2002**, *35*, 565−573.
(67) Lewis, T. C.; Tocher, D. A.; Price, S. L. *Cryst. Growth Des.* **2005**, *5*, 983−993.

evidence of a dimer-based polymorph but cannot exclude further polymorphs being found by other crystallization methods that have recently been shown to generate new forms, such as polymer templating,[68] crystallization additives,[69,70] or in the course of attempted cocrystallization experiments.[71] This screen produced two solvates, the known unsolvated form, a metastable polymorph, and a plastic crystalline phase. While the plastic phase is stable above 145 °C, the catemer-based form 1 is the most stable known polymorph at ambient temperatures, and is almost certainly the most stable possible structure down to 0 K.

The relative energies of potential crystal structures of **I** implies that such a dimer-based polymorph would be within the possible energy range of potential polymorphs, though no evidence of such a form has been found. This can be rationalized in terms of the unusual balance between the hydrogen bonding and van der Waals interactions of this nearly spherical molecule, allowing the facile rearrangement of nucleating clusters containing the dimer into the more stable hydrogen bonded chain-based form. The evidence that there is at most a low kinetic barrier to the rearrangement of clusters of dimers into a catemer-based motif reduces the likelihood that any crystallization method could achieve a new dimer-based polymorph of **I**.

This study clearly demonstrates the synergy between experimental polymorph screening and the computational prediction of the energetically feasible crystal structures and reinforces the recognition[40] that a more complete understanding of the kinetic, thermodynamic, and structural aspects of nucleation is required for further development of computational polymorph prediction methodologies.

Acknowledgment. G. M. Day, R. J. Davey, and G. Dent are thanked for valuable discussions, and G. M. Day is thanked for providing the results of his computational study. The authors acknowledge the Basic Technology Program of the Research Councils UK for supporting "Control and Prediction of the Organic Solid State" (www.cposs.org.uk Grant Number GR/S24114/01 to S.L.P.).

Supporting Information Available: Computed crystal structures are stored on CCLRC e-Science Centre dataportal and are available from the authors on request. The following Supporting Information is available: S1 Details of synthesis; S2 Spectroscopic investigation of solution aggregation; S3 Crystal Structure Prediction results; S4 Principal Component Analysis of solvent molecules; S5 Crystallization details, results, and XRPD analysis; S6 Overlay diagram contrasting forms 1 and 2; S7 Ab initio optimized geometry and energy for **I**; S8 Complete refs 3, 4, and 14. This material is available free of charge via the Internet at http://pubs.acs.org.

JA0687466

(68) Price, C. P.; Grzesiak, A. L.; Matzger, A. J. *J. Am. Chem. Soc.* **2005**, *127*, 5512−5517.
(69) Weissbuch, I.; Addadi, L.; Lahav, M.; Leiserowitz, L. *Science* **1991**, *253*, 637−645.
(70) Torbeev, V. Y.; Shavit, E.; Weissbuch, I.; Leiserowitz, L.; Lahav, M. *Cryst. Growth Des.* **2005**, *5*, 2190−2196.
(71) Day, G. M.; Trask, A. V.; Motherwell, W. D. S.; Jones, W. *Chem. Commun.* **2006**, 54−56.